A Simulation Framework for RIS Communications

Jonathan W. Browing[1], Nidhi Simmons[1], Paschalis C. Sofotasios[2,3], Simon L. Cotton[1],
David Morales-Jimenez[4], Michail Matthaiou[1], and Muhammad Ali Babar Abbasi[1]
[1]Centre for Wireless Innovation, ECIT Institute, Queen's University Belfast, BT3 9DT, Belfast, UK
[2]Center for Cyber Physical Systems, EECS Department, Khalifa University, 127788, Abu Dhabi, UAE
[3]Department of Electrical Engineering, Tampere University, 33101, Tampere, Finland
[4]Department of Signal Theory, Telematics and Communications, University of Granada, 18071, Granada, Spain

2023 IEEE 97th Vehicular Technology Conference (VTC2023-Spring) | 979-8-3503-1114-3/23/$31.00 ©2023 IEEE | DOI: 10.1109/VTC2023-Spring57618.2023.10199925

***Abstract*—This contribution proposes a simulation framework for quantifying the performance of employed reconfigurable intelligent surface (RIS) based systems to overcome adverse propagation-related effects. The physical model underlying the proposed framework considers the presence of a dominant signal path between the source and RIS, and then between RIS and the destination. The simulation of the time-correlated scattered signal reflected by the illuminated reflective elements is achieved using autoregressive (AR) modeling. As a by-product of our analysis, significant insights are developed which allow for the characterization of the amplitude and phase properties of the received signal, and the associated complex autocorrelation function (ACF) for the product of two Rician channels. Capitalizing on this, we derive the corresponding first and second order statistics, which lead to the development of useful theoretical and practical insights.**

I. Introduction

To truly enable the next generation of wireless technologies, such as enhanced mobile broadband (eMBB), ultra-reliable low-latency communication (uRLLC), and massive machine-type communication (mMTC), calls for a major shift in the network infrastructure paradigm [1], [2]. One potential approach is the utilization of intelligent meta-surfaces [3], which are two-dimensional planar arrays composed of a high number of passive reflective meta-atoms/antennae (hereby referred to as elements) that are on the order of sub-wavelengths of the operating frequency [4], [5]. The reflective elements within a meta-surface can be controlled to alter their reflective properties in order to manipulate the propagation of any signals which are impinged upon them [6]. As a result, this property allows the control of phase shifts applied by each of the reflective elements [7]. By distributing these smart surfaces throughout a network, operators will be able to overcome unfavorable propagation phenomena in cellular environments [8], [9], in a cost effective manner [**?**].

In the literature, the same technology has been referred to as software-controlled metasurfaces [8], intelligent reflective surfaces [10]–[12] or reconfigurable intelligent surfaces (RISs) [13]–[15] whilst a number of studies have investigated the theoretical performance of RISs in recent years [12], [16]–[22]. However, unlike the theoretical treatment of performance analysis, the simulation of RIS systems has received less attention, despite its importance for providing insights into the system performance in the presence of spatio-temporal variations. With this motivation, this contribution develops a simulation framework, which is built upon underlying Gaussian random variables (RVs), for wireless transmission from a source to destination through multiple cooperative RISs. Through our analysis, we were able to obtain expressions for a number of the first- and second-order statistics associated with product (or equivalently cascaded) complex Rician channels, including the complex autocorrelation function (ACF). The latter enables us to account for important channel properties through each of the cascaded links, such as potential Doppler effects, a dominant signal component, and a *non-isotropic* scattered signal contribution, which caters for angular selectivity. By further exploiting the complex ACF and the properties of the fading model, we harness the power of autoregressive (AR) modeling [23] to implement our simulator. We recall that AR modeling has previously been successfully used for channel prediction and the simulation of correlated Rayleigh and Nakagami-m fading channels [23], [24].

II. Physical Model

We consider a single RIS case and the optional presence of dominant signal paths between the source and the RIS and then between the RIS and the destination. Accompanying this is a scattered signal contribution which can be modeled as a zero-mean complex Gaussian random process [10]. As shown later, the scattered signal for RISs may exhibit non-isotropic transmission and reception behavior. Furthermore, each stage of the cascaded channel can be denoted in vector form as $\mathbf{p} = [p_1, \ldots, p_l, \ldots, p_L]^T$ and $\mathbf{g} = [g_1, \ldots, g_l, \ldots, g_L]^T$, where T denotes the transpose operator. Following from this, the l^{th} illuminated reflective elements of both $\mathbf{p}$ and $\mathbf{g}$ are characterized as complex non-zero mean Gaussian RVs due to the superposition of the dominant and scattered signal contributions within each cascaded stage of the source-to-destination link. Therefore, the magnitudes of the l^{th} illuminated reflective elements of both $\mathbf{p}$ and $\mathbf{g}$ follow the Rician distribution [25].

The complex signal envelope at the destination is denoted as $S = R\exp(j\Theta)$, where R is the received signal envelope and Θ is the received signal phase. Also, the in-phase and quadrature components are represented by X and Y, respectively. Based on this, it follows that $S = X + jY$, $R^2 = X^2 + Y^2$, $\Theta = \arg(X + jY)$, $X = R\cos(\Theta)$ and $Y = R\sin(\Theta)$. Also, sub index $\lambda = 1$ refers to the path between the source and the RIS for each illuminated reflective element (i.e., p_l). Correspondingly, sub index $\lambda = 2$ refers

to the path between the RIS and the destination for each illuminated reflective element (i.e., g_l). Letting the quadrature components, which make up the signal contribution from each illuminated reflected element, be represented by complex non-zero mean Gaussian RVs, the received signal power at the destination can now be expressed as

$$R^2 = \sum_{l=1}^{L} \prod_{\lambda=1}^{2} \left[(B_{\lambda,l} + u_{\lambda,l})^2 + (C_{\lambda,l} + v_{\lambda,l})^2 \right], \quad (1)$$

where L is the number of illuminated reflective elements, and $B_{\lambda,l}$ and $C_{\lambda,l}$ are mutually independent Gaussian RVs with $\mathbb{E}[B_{\lambda,l}] = \mathbb{E}[C_{\lambda,l}] = 0$ and $\mathbb{E}[B_{\lambda,l}^2] = \mathbb{E}[C_{\lambda,l}^2] = \sigma_{\lambda,l}^2$, with $\mathbb{E}$ denoting statistical expectation. The time-varying amplitudes of the in-phase and quadrature components of the dominant signal component are represented by $u_{\lambda,l}$ and $v_{\lambda,l}$, respectively, with the variation related to the embedded Doppler effect [26]. Also, the Rician $k_{\lambda,l}$ factor represents the ratio between the total power of the dominant signal component, $\delta_{\lambda,l}^2 = u_{\lambda,l}^2 + v_{\lambda,l}^2$, and the total power of the scattered signal component $2\sigma_{\lambda,l}^2$, where $\sigma_{\lambda,l} = \bar{r}_{\lambda,l}/\sqrt{2(1+k_{\lambda,l})}$, with $\bar{r}_{\lambda,l} = \sqrt{\mathbb{E}[R_{\lambda,l}^2]}$ denoting the root mean square (rms) of the signal envelope. Based on this, it follows that $k_{\lambda,l} = u_{\lambda,l}^2 + v_{\lambda,l}^2/(2\sigma_{\lambda,l}^2)$, while by defining $\varpi_{\lambda,l} = \arg(u_{\lambda,l} + j v_{\lambda,l})$ as a phase parameter one obtains

$$\left\{ \frac{u_{\lambda,l}}{v_{\lambda,l}} \right\} = \sqrt{\frac{k_{\lambda,l}}{1+k_{\lambda,l}}} \bar{r}_{\lambda,l} \left\{ \frac{\cos(\varpi_{\lambda,l})}{\sin(\varpi_{\lambda,l})} \right\}. \quad (2)$$

If only one reflective element is illuminated (i.e., $L = 1$ and the l subindex is omitted), the model in (1) simplifies to

$$R^2 = \prod_{\lambda=1}^{2} \left[(B_\lambda + u_\lambda)^2 + (C_\lambda + v_\lambda)^2 \right]. \quad (3)$$

III. Product of Rician channels

Based on the above, we now present new results for the product of two Rician channels.

1) First-Order Statistics: Considering the model in (3), the PDF of the received signal envelope, R, for the product of two complex Rician channels is given by [27, Eq. (19)], which is fully convergent. Of note, knowledge of the received signal phase is essential for the accurate characterization of complex channels and the design of phase-based modulation schemes [28], [29]. Nevertheless, the PDF of the received signal phase for the product of two complex Rician channels has not been reported in the open literature. This is derived next.

Theorem 1. *For $\{k_1, k_2\} \in \mathbb{R}_{\geq 0}$, $\{\varpi_1, \varpi_2, \theta\} \in [-\pi, \pi]$ the PDF of the received signal phase in (3), which considers the product of two complex Rician channels, is expressed as*

$$f_\Theta(\theta) = \sum_{b,c,d=0}^{\infty} \frac{\exp(-k_1) k_1^c k_2^b \Gamma\left(b+1+\frac{d}{2}\right) \Gamma\left(c+1+\frac{d}{2}\right)}{2\pi \exp(k_2) b! c! d! \Gamma(b+c+1)(b+c+1)_d} \times \left(2\sqrt{k_1 k_2} \cos(\theta - \varpi_1 - \varpi_2) \right)^d. \quad (5)$$

Proof: The PDF of the received signal phase for the product of two complex Rician channels is found by integrating the joint envelope-phase distribution with respect to the received signal envelope, R. The product of two independent non-zero mean complex Gaussians is given by [27, Eq. (6)], namely

$$f_{R,\Theta}(r,\theta) = \sum_{b,c=0}^{\infty} \frac{2r \exp\left(-k_1^2 - k_2^2\right) \beta^{b+c}}{\pi \sigma_1^2 \sigma_2^2 \left(2\cos\theta - \phi_1\phi_2\right)^{b+c}} \frac{I_{b+c}(2\beta)}{b!c!} \times \left(\frac{k_1}{k_2} \right)^{b-c} K_{b-c}\left(\frac{2r}{\sigma_1\sigma_2} \right), \quad (6)$$

where $\beta = \sqrt{2rk_1k_2\cos(\theta - \phi_1 - \phi_2)/\sigma_1\sigma_2}$, and corresponds to the joint envelope-phase distribution of (3). By substituting $\sigma_1 = \bar{r}_1/\sqrt{2(1+k_1)}$ and $\sigma_2 = \bar{r}_2/\sqrt{2(1+k_2)}$ and then integrating with respect to the received signal envelope using the identities [30, Eq. (03.02.06.0037.01)] and [31, Eq. (6.561.16)] yields (5), which completes the proof. □

2) Second-Order Statistics: The backbone of our proposed simulation framework is the use of AR modeling to induce the time variant properties of the fading into the complex Gaussian RVs underlying each of the cascaded stages of transmission. Central to the construction of the appropriate AR model for channel simulation in our proposed framework is the knowledge of the associated complex ACF. This requires expansion of the physical model to include other propagation related effects, not apparent within the first-order statistics. To this effect, we consider the product of two complex Rician channels in (3), which accounts for the case when only one reflective element is illuminated for a single RIS-assisted transmission. For ease of understanding, and to remove any potential ambiguity, we let $\delta_\lambda(t)$ represent the complex amplitude of the dominant signal component, and $\varrho_\lambda(t)$ account for the scattered signal component in each of the complex Gaussian RVs in $\mathbf{p}$ and $\mathbf{g}$. The time dependent complex received signal for a single Rician channel is already known as in [32]. Hence, for the product of two Rician channels case it follows that

$$S(t) = \prod_{\lambda=1}^{2} \frac{\bar{r}_\lambda \left[\varrho_\lambda(t) + \sqrt{k_\lambda}\delta_\lambda(t) \right]}{\sqrt{1+k_\lambda}}, \quad (7)$$

where $\bar{r}_\lambda$ and k_λ have been defined previously. When $\lambda = 1$, (7) represents the first stage of transmission which occurs between the source and the RIS, whereas when $\lambda = 2$, this denotes the second stage of transmission which occurs between the RIS and the destination. We also let $f_{\delta\lambda}$ and $\alpha_{\delta\lambda}$ represent the relative Doppler frequency and the DoA of the dominant signal component, respectively. Using [33], the dominant signal component, $\delta_\lambda(t)$, is expressed as $\exp\left(j\left(2\pi f_{\delta\lambda} t \cos\left(\alpha_{\delta\lambda}\right) + \varphi_{0\lambda}\right)\right)$ where, $\varphi_{0\lambda}$, is the initial phase, uniformly distributed on the interval $[-\pi, \pi]$. Now by adopting the notation provided in [34, p. 82] the scattered signal contribution, $\varrho_\lambda(t)$, can be represented as

$$\varrho_\lambda(t) = \sum_{q=1}^{\mathcal{Q}} \frac{e^{j2\pi t\left(f_{D\lambda}\cos\left(\alpha_{q,D\lambda}\right) + f_{A\lambda}\cos\left(\alpha_{q,A\lambda}\right)\right) + j\varphi_{q\lambda}}}{\mathcal{Q}}, \quad (8)$$

$$f_R(r) = \sum_{b,c=0}^{\infty} \frac{4rk_1^b k_2^c (1+k_1)(1+k_2)\exp(-k_1-k_2)}{\bar{r}_1^2 \bar{r}_2^2 \Gamma(b+1)\Gamma(c+1)\, b!c!} \left(\frac{r\sqrt{(1+k_1)(1+k_2)}}{\bar{r}_1\bar{r}_2}\right)^{b+c} K_{c-b}\left(\frac{2r\sqrt{(1+k_1)(1+k_2)}}{\bar{r}_1\bar{r}_2}\right) \quad (4)$$

where $\mathcal{Q}$ is the number of propagation paths, $f_{D\lambda}$ and $f_{A\lambda}$ are the maximum Doppler frequencies of the signal departing from the source and arriving at the RIS (i.e., f_{D1} and f_{A1}), and departing from the RIS and arriving at the destination (i.e., f_{D2} and f_{A2}), respectively. The Doppler shifts observed in a RIS system can occur for multiple reasons, such as the mobility of the source and destination, mobile scatterers in the local environment, or some combination thereof. The random direction of departure (DoD) of the q^{th} propagation path with reference to the respective velocity vector is α_{q,D_λ}, while α_{q,A_λ} is the random direction of arrival (DoA). The variable φ_{q_λ} is a random phase uniformly distributed on $[-\pi,\pi]$ and is independent of α_{q,D_λ} and α_{q,A_λ} for all q. This reference model allows greater flexibility in considering either or both ends of the transmission to be in motion [34, p. 82].

It is noted here that since the RISs can be deployed in urban environments to assist transmission to users in blind zones [9], the scattered signal component may be subject to spatial filtering and as a consequence be non-isotropic in nature [35]. In this case, the distribution of the DoD or DoA of the scattered signal component can be modeled using the versatile Von Mises distribution [36]. This distribution can be used to model propagation scenarios in which the DoD or DoA of multipath waves are either isotropic or non-isotropic. The Von Mises distribution for the DoD (or DoA) of the scattered signal contributions, $f_{\mathcal{A}\lambda}(\alpha_\lambda)$, is given by [36]

$$f_{\mathcal{A}\lambda}(\alpha_\lambda) = \frac{\exp(\kappa_\lambda \cos(\alpha_\lambda - \bar{\alpha}_\lambda))}{2\pi I_0(\kappa_\lambda)}, \quad (9)$$

where $\alpha_\lambda \in [-\pi,\pi]$, $\kappa_\lambda \geq 0$ controls the spread of the DoD ($\kappa_{D\lambda}$) and the DoA ($\kappa_{A\lambda}$). The mean DoD or DoA are accounted for by $\bar{\alpha}_{D\lambda}$ and $\bar{\alpha}_{A\lambda}$, respectively, and each can take values in the range $[-\pi,\pi]$. When $\kappa_\lambda = 0$, (9) reduces to the circular uniform distribution and the signal received is the result of isotropic scattering. As κ_λ increases, the DoD or DoA becomes increasingly unidirectional with $\kappa_\lambda \to \infty$ describing extremely non-isotropic scattering. As discussed in [36], a useful estimator of the spread of the DoD or DoA in polar coordinates for increasing values of κ_λ (i.e., $\kappa_\lambda > 1$) can be obtained by considering the inflection points of $f_{\mathcal{A}\lambda}(\alpha_\lambda)$ which are approximately equal to $\pm 1/\sqrt{\kappa_\lambda}$. For highly non-isotropic scattering, e.g., for $\kappa_\lambda = 3$ and 5, the spread of the DoD or DoA of these contributions can be estimated as $2/\sqrt{\kappa_\lambda}$, giving 66° and 51°, respectively.

Using the previous definition of the dominant signal component, $\delta_\lambda(t)$, and the scattered signal component, $\varrho_\lambda(t)$, the complex ACF with respect to the time lag, τ, of the model given in (7) is now presented by the following Theorem.

Theorem 2. *For* $\{k_\lambda, \tau, f_{\delta\lambda}, f_{D\lambda}, \kappa_{D\lambda}, f_{A\lambda}, \kappa_{A\lambda}\} \in \mathbb{R}_{\geq 0}$, $\{\bar{r}_\lambda\} \in \mathbb{R}_{>0}$, $\{\alpha_{\delta\lambda}, \bar{\alpha}_{D\lambda}, \bar{\alpha}_{A\lambda}\} \in [-\pi,\pi]$, *the complex ACF of the model for the product of two Rician channels in (7) can be expressed as in* (10).

Proof: The ACF of a wide sense stationary process may be written as $\phi_{SS}(\tau) = \mathbb{E}[S(t)S^*(t+\tau)]$, where t is the current time and τ is the time lag [34]. Using (7) as a model for the complex received signal when one reflective element is illuminated and after some mathematical manipulations, the complex ACF may be expressed as $\phi_{SS}(\tau) = \prod_{\lambda=1}^{2} \frac{\bar{r}_\lambda^2}{1+k_\lambda} \mathbb{E}\left[(\varrho_\lambda(t)\varrho_\lambda^*(t+\tau) + k_\lambda \exp(j2\pi f_{\delta\lambda}\tau\cos(\alpha_{\delta\lambda})))\right]$. Evaluating the autocorrelation of the scattered signal component separately for each complex Gaussian RV yields (11), which conveniently reduces to

$$\phi_{\varrho_\lambda\varrho_\lambda}(\tau) = \lim_{\mathcal{Q}\to\infty} \sqrt{\frac{1}{\mathcal{Q}}} \sum_{q=1}^{\mathcal{Q}} \mathbb{E}\left[\exp\left(j2\pi f_{D\lambda}\tau\cos\left(\alpha_{q,D_\lambda}\right)\right) \times \exp\left(j2\pi f_{A\lambda}\tau\cos\left(\alpha_{q,A_\lambda}\right)\right)\right]. \quad (12)$$

Knowing that $\alpha_{D\lambda}$ and $\alpha_{A\lambda}$ are independent RVs ($\mathbb{E}[\alpha_{D\lambda}\alpha_{A\lambda}] = \mathbb{E}[\alpha_{D\lambda}]\mathbb{E}[\alpha_{A\lambda}]$), followed by substituting the PDF given in (9) into (12) along with [31, Eq. (3.338.4)], yields (13). By substituting (13) yields the complex ACF in (10), which completes the proof. □

The derived complex ACF in (10) is a general expression for both isotropic (i.e., $\kappa_{D\lambda} = 0$ or $\kappa_{A\lambda} = 0$) and non-isotropic (i.e., $\kappa_{D\lambda} > 0$ or $\kappa_{A\lambda} > 0$) scattering conditions that can occur between the source and the RIS, and then between the RIS and the destination. It is also recalled that it is often more convenient to use the complex ACF in its normalized form, given by $\tilde{\phi}_{SS}(\tau)$. This can be straightforwardly obtained by setting $\bar{r}_\lambda = 1$ in (10).

sAcknowledgments*

IV. Numerical Results

It is noted that several propagation scenarios arise from the model in (3), which have a significant impact on the properties of the received signal phase. Figure 1 illustrates the form of the PDF of the received signal phase for a number of propagation scenarios of interest. Firstly, as expected, we observe that when $k_1 = k_2 = 0$, the received signal phase follows the circular uniform distribution. Most strikingly, when only one of the Gaussian RVs has a zero mean, it is found that the resultant received signal phase is still uniformly distributed, which is consistent with the result presented in [37]. This observation suggests that the clustering of the signals around a particular phase, which is introduced by the dominant signal component in one stage of the cascaded transmission, is diffused in the

$$\phi_{SS}(\tau)=\prod_{\lambda=1}^{2}\frac{\bar{r}_{\lambda}^{2}}{(1+k_{\lambda})}\left[\frac{(I_0(\kappa_{D\lambda}))^{-1}I_0\left(\sqrt{\kappa_{A\lambda}^2-4\pi^2 f_{A\lambda}^2\tau^2+j4\pi\kappa_{A\lambda}\cos(\bar{\alpha}_{A\lambda})f_{A\lambda}\tau}\right)}{\left(I_0\left(\sqrt{\kappa_{D\lambda}^2-4\pi^2 f_{D\lambda}^2\tau^2+j4\pi\kappa_{D\lambda}\cos(\bar{\alpha}_{D\lambda})f_{D\lambda}\tau}\right)\right)^{-1}I_0(\kappa_{A\lambda})}+k_{\lambda}e^{(j2\pi f_{\delta\lambda}\tau\cos(\alpha_{\delta\lambda}))}\right] \tag{10}$$

$$\phi_{\varrho_\lambda\varrho_\lambda}(\tau)=\lim_{\mathcal{Q}\to\infty}\sqrt{\frac{1}{\mathcal{Q}}}\sum_{q=1}^{\mathcal{Q}}\mathbb{E}\left[\exp\left\{\begin{array}{l}j\left(2\pi f_{D\lambda}t\cos\left(\alpha_{q,D_\lambda}\right)+2\pi f_{A\lambda}t\cos\left(\alpha_{q,A_\lambda}\right)+\varphi_{q,\lambda}\right)\\-j\left(2\pi f_{D\lambda}(t+\tau)\cos\left(\alpha_{q,D_\lambda}\right)\right.\\+2\pi f_{A\lambda}\left(t+\tau\right)\cos\left(\alpha_{q,A_\lambda}\right)+\varphi_{q,\lambda}\end{array}\right\}\right] \tag{11}$$

$$\phi_{\varrho_\lambda\varrho_\lambda}(\tau)=\frac{\left(I_0\left(\kappa_{D\lambda}\right)\right)^{-1}I_0\left(\sqrt{\kappa_{A\lambda}^2-4\pi^2 f_{A\lambda}^2\tau^2+j4\pi\kappa_{A\lambda}\cos\left(\bar{\alpha}_{A\lambda}\right)f_{A\lambda}\tau}\right)}{\left(I_0\left(\sqrt{\kappa_{D\lambda}^2-4\pi^2 f_{D\lambda}^2\tau^2+j4\pi\kappa_{D\lambda}\cos\left(\bar{\alpha}_{D\lambda}\right)f_{D\lambda}\tau}\right)\right)^{-1}I_0\left(\kappa_{A\lambda}\right)}. \tag{13}$$

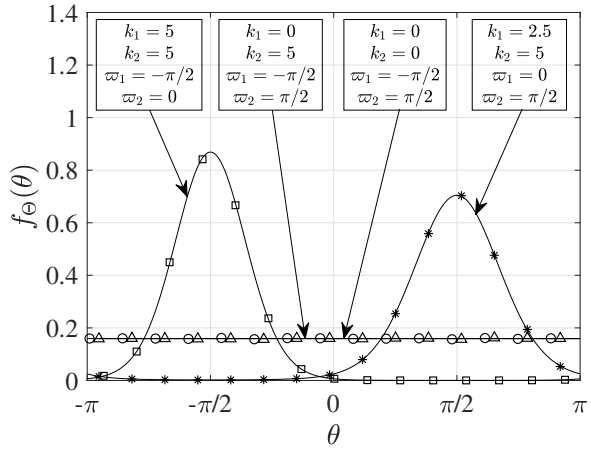

Fig. 1. The PDF of the received signal phase of the product of two complex Rician channels in (5) for varying cases. The lines represent analytical results, with a maximum number of terms of $b=c=d=15$, while the shapes represent the results of the Monte-Carlo simulations using 1×10^6 samples for each stage of the transmission.

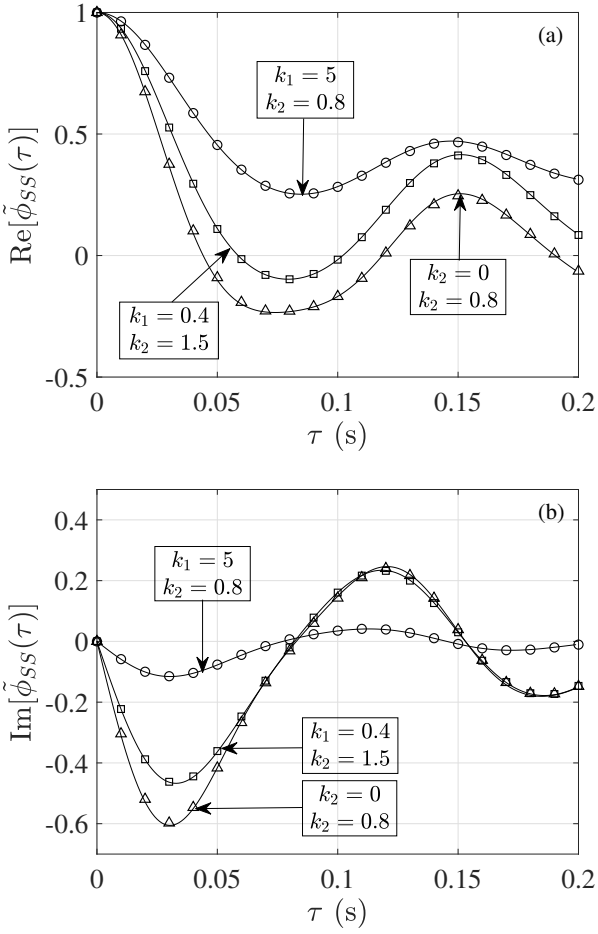

Fig. 2. The normalized complex ACF of a single RIS system with one illuminated reflective element (lines) in (10) alongside simulation results using an AR model order of 200 (shapes) for varying k_1 and k_2, with $\varpi_1=\varpi_2=\pi/4$ rad, $f_{\delta1}=f_{\delta2}=0$ Hz, $\alpha_{\delta1}=\alpha_{\delta2}=0$ rad, $\kappa_{D1}=2,\kappa_{D2}=4,f_{D1}=7$ Hz, $f_{D2}=0.3$ Hz, $\bar{\alpha}_{D1}=-\pi$ rad, $\bar{\alpha}_{D2}=\pi$ rad, $\kappa_{A1}=4,\kappa_{A2}=2,f_{A1}=0.2$ Hz, $f_{A2}=8$ Hz, $\bar{\alpha}_{A1}=\pi$ rad, and $\bar{\alpha}_{A2}=\pi/2$ rad: (a) the real part and (b) the imaginary part.

other stage of transmission. When both Gaussian RVs have non-zero means, both Rician k factors control the concentration of the distribution around the maximum, which occurs at $\theta=\varpi_1+\varpi_2$, while the minima is located at $\theta=\varpi_1+\varpi_2+\pi$.

As an example, now let us consider the real and imaginary parts of the complex ACF for the case where a source transmits to a RIS, illuminating a single reflective element, and the RIS reflects the signal to the destination. The real part of the normalized ACF for this type of scenario is given in Fig. 2(a). It can be seen that when either k_1 or k_2 are decreased, there is weaker correlation, as compared to the case where there is at least one strong dominant signal component present (e.g., $k_1=5$ and $k_2=0.8$). Next, we compare the real part in Fig. 2(a) to the imaginary part in Fig. 2(b), which is a measure of the cross-correlation of the real and imaginary parts of the complex received signal [34]. We observe that in the presence of stronger dominant signal components, there is greater correlation between the two quadrature components in this particular example, where the scattering conditions have

remained identical.

V. Conclusion

We presented a physical model for single RIS-assisted transmission with the fluctuation of the signal transmitted between the reflective elements assumed to follow the Rician fading distribution. Based on the physical models, novel formulations for the PDF of the received signal phase were provided for the product of two complex Rician channels. A number of examples have been included for the PDF of the received signal phase alongside respective simulated results to demonstrate its validity. To facilitate the simulation of cooperative RIS-assisted transmission, the complex ACF of the signal reflected by each illuminated reflective element was obtained, taking into account non-isotropic transmission and Doppler effects caused by mobility and/or the environment. Thanks to the physical model being fully defined in terms of underlying Gaussian RVs, introduction of temporal correlation within our framework was achieved using AR-based simulation, utilizing the derived complex ACF. Finally, besides RIS systems, the proposed model can be used to simulate a wide variety of wireless systems such as relay or metasurface assisted communications, D2D and point-to-point communications, which make use of antenna arrays and cascaded links.

References

[1] M. Matthaiou, O. Yurduseven, H. Q. Ngo, D. Morales-Jimenez, S. L. Cotton, and V. F. Fusco, "The road to 6G: Ten physical layer challenges for communications engineers," *IEEE Commun. Mag.*, vol. 59, no. 1, pp. 64–69, Jan. 2021.

[2] J. Zhang, E. Björnson, M. Matthaiou, D. W. K. Ng, H. Yang, and D. J. Love, "Prospective multiple antenna technologies for beyond 5G," *IEEE J. Sel. Areas Commun.*, vol. 38, no. 8, pp. 1637–1660, Aug. 2020.

[3] Q. Wu, S. Zhang, B. Zheng, C. You, and R. Zhang, "Intelligent reflecting surface aided wireless communications: A tutorial," *IEEE Trans. Commun.*, vol. 69, no. 5, pp. 3313–3351, May 2021.

[4] D. Headland *et al.*, "Terahertz reflectarrays and nonuniform metasurfaces," *IEEE J. Sel. Topics Quantum Electron.*, vol. 23, no. 4, pp. 1–18, Jul. 2017.

[5] N. Mohammadi Estakhri and A. Alù, "Wave-front transformation with gradient metasurfaces," *Phys. Rev. X*, vol. 6, no. 4, p. 041008, Oct. 2016. [Online]. Available: https://link.aps.org/doi/10.1103/PhysRevX.6.041008

[6] M. D. Renzo *et al.*, "Smart radio environments empowered by reconfigurable AI meta-surfaces: An idea whose time has come," *EURASIP J. Wireless Commun. Netw.*, vol. 2019, no. 1, p. 129, May 2019.

[7] T. J. Cui, M. Q. Qi, X. Wan, J. Zhao, and Q. Cheng, "Coding metamaterials, digital metamaterials and programmable metamaterials," *Light: Science & Applications*, vol. 3, no. 10, Oct. 2014.

[8] C. Liaskos, S. Nie, A. Tsioliaridou, A. Pitsillides, S. Ioannidis, and I. Akyildiz, "A new wireless communication paradigm through software-controlled metasurfaces," *IEEE Commun. Mag.*, vol. 56, no. 9, pp. 162–169, Sep. 2018.

[9] Q. Wu and R. Zhang, "Towards smart and reconfigurable environment: Intelligent reflecting surface aided wireless network," *IEEE Commun. Mag.*, vol. 58, no. 1, pp. 106–112, Jan. 2020.

[10] ——, "Intelligent reflecting surface enhanced wireless network via joint active and passive beamforming," *IEEE Trans. Wireless Commun.*, vol. 18, no. 11, pp. 5394–5409, Nov. 2019.

[11] M. Cui, G. Zhang, and R. Zhang, "Secure wireless communication via intelligent reflecting surface," *IEEE Wireless Commun. Lett.*, vol. 8, no. 5, pp. 1410–1414, Oct. 2019.

[12] E. Björnson, Ö. Özdogan, and E. G. Larsson, "Intelligent reflecting surface versus decode-and-forward: How large surfaces are needed to beat relaying?" *IEEE Wireless Commun. Lett.*, vol. 9, no. 2, pp. 244–248, Feb. 2020.

[13] C. Huang, A. Zappone, G. C. Alexandropoulos, M. Debbah, and C. Yuen, "Reconfigurable intelligent surfaces for energy efficiency in wireless communication," *IEEE Trans. Wireless Commun.*, vol. 18, no. 8, pp. 4157–4170, Aug. 2019.

[14] E. Basar, "Reconfigurable intelligent surface-based index modulation: A new beyond MIMO paradigm for 6G," *IEEE Trans. Commun.*, vol. 68, no. 5, pp. 3187–3196, May 2020.

[15] L. Dai *et al.*, "Reconfigurable intelligent surface-based wireless communications: Antenna design, prototyping, and experimental results," *IEEE Access*, vol. 8, pp. 45 913–45 923, 2020.

[16] Y. Han, S. Zhang, L. Duan, and R. Zhang, "Cooperative double-IRS aided communication: Beamforming design and power scaling," *IEEE Wireless Commun. Lett.*, vol. 9, no. 8, pp. 1206–1210, Aug. 2020.

[17] M. Jung, W. Saad, Y. Jang, G. Kong, and S. Choi, "Reliability analysis of large intelligent surfaces (LISs): Rate distribution and outage probability," *IEEE Wireless Commun. Lett.*, vol. 8, no. 6, pp. 1662–1666, Dec. 2019.

[18] T. Bai, C. Pan, Y. Deng, M. Elkashlan, A. Nallanathan, and L. Hanzo, "Latency minimization for intelligent reflecting surface aided mobile edge computing," *IEEE J. Sel. Areas Commun.*, vol. 38, no. 11, pp. 2666–2682, Nov. 2020.

[19] M.-A. Badiu and J. P. Coon, "Communication through a large reflecting surface with phase errors," *IEEE Wireless Commun. Lett.*, vol. 9, no. 2, pp. 184–188, Feb. 2020.

[20] Q. Nadeem, H. Alwazani, A. Kammoun, A. Chaaban, M. Debbah, and M. Alouini, "Intelligent reflecting surface-assisted multi-user MISO communication: Channel estimation and beamforming design," *IEEE Open J. Commun. Soc.*, vol. 1, pp. 661–680, May 2020.

[21] W. Yan, X. Yuan, and X. Kuai, "Passive beamforming and information transfer via large intelligent surface," *IEEE Wireless Commun. Lett.*, vol. 9, no. 4, pp. 533–537, Apr. 2020.

[22] D. Kudathanthirige, D. Gunasinghe, and G. Amarasuriya, "Performance analysis of intelligent reflective surfaces for wireless communication," in *Proc. IEEE ICC*, Jun. 2020, pp. 1–6.

[23] K. E. Baddour and N. C. Beaulieu, "Autoregressive modeling for fading channel simulation," *IEEE Trans. Wireless Commun.*, vol. 4, no. 4, pp. 1650–1662, Jul. 2005.

[24] J. C. S. Santos, M. D. Yacoub, and G. Fraidenraich, "A simple accurate method for generating autocorrelated Nakagami-m envelope sequences," *IEEE Commun. Lett.*, vol. 11, no. 3, pp. 231–233, Mar. 2007.

[25] S. O. Rice, "Statistical properties of a sine wave plus random noise," *Bell Syst. Tech. J.*, vol. 27, no. 1, pp. 109–157, Jan. 1948.

[26] T. Aulin, "A modified model for the fading signal at a mobile radio channel," *IEEE Trans. Veh. Technol.*, vol. 28, no. 3, pp. 182–203, Aug. 1979.

[27] N. O'Donoughue and J. M. F. Moura, "On the product of independent complex Gaussians," *IEEE Trans. Signal Process.*, vol. 60, no. 3, pp. 1050–1063, Mar. 2012.

[28] D. Hess, "Cycle slipping in a first-order phase-locked loop," *IEEE Trans. Commun. Technol.*, vol. 16, no. 2, pp. 255–260, Apr. 1968.

[29] J. G. Proakis, *Digital Communications*, 4th ed. New York: McGraw-Hill, 2001.

[30] "Wolfram Research, Inc." accessed on 03/25/2019. [Online]. Available: http://functions.wolfram.com/

[31] I. S. Gradshteyn and I. M. Ryzhik, *Table of Integrals, Series, and Products*, 7th ed. San Diego, CA, USA: Academic Press, 2007.

[32] K. Baddour and N. Beaulieu, "Accurate simulation of multiple cross-correlated Rician fading channels," *IEEE Trans. Commun.*, vol. 52, no. 11, pp. 1980–1987, Nov. 2004.

[33] L. Wang, W. Liu, and Y. Cheng, "Statistical analysis of a mobile-to-mobile Rician fading channel model," *IEEE Trans. Veh. Technol.*, vol. 58, no. 1, pp. 32–38, Jan. 2009.

[34] G. L. Stüber, *Principles of Mobile Communication*, 3rd ed. Springer, 2011.

[35] B. N. Liya and D. G. Michelson, "Characterization of multipath persistence in device-to-device scenarios at 30 GHz," in *Proc. IEEE GLOBECOM*, Dec. 2016, pp. 1–6.

[36] A. Abdi, J. A. Barger, and M. Kaveh, "A parametric model for the distribution of the angle of arrival and the associated correlation function and power spectrum at the mobile station," *IEEE Trans. Veh. Technol.*, vol. 51, no. 3, pp. 425–434, May 2002.

[37] F. Scire, "A probability density function theorem for the modulo y values of the sum of two statistically independent processes," *Proc. IEEE*, vol. 56, no. 2, pp. 204–205, Feb. 1968.